Morphology of Carbon Supported Pt−Ru Electrocatalyst and the CO Tolerance of Anodes for PEM Fuel Cells

Shawn D. Lin and Ting-Chou Hsiao

Department of Chemical Engineering, Yuan Ze University, Chung-Li, Taiwan, R.O.C

Jen-Ray Chang

Department of Chemical Engineering, National Chung Cheng University, Chia-Yi, Taiwan, R.O.C

Andrew S. Lin*

Energy and Resource Laboratories, Industrial Technology Research Institute, Hsinchu, Taiwan, R.O.C

Received: May 19, 1998; In Final Form: October 8, 1998

Two Pt−Ru/C catalysts, a commercial 20% Pt−10% Ru/C and a 10% Pt−5% Ru/C synthesized in house (YZU catalyst), were examined for the CO tolerance in polymer-electrolyte-membrane fuel cells (PEFCs). Both half-cell tests under 250 ppm of CO/H_2 and single-cell tests under 100 ppm of CO/H_2 showed that the YZU catalyst had smaller increase in the overvoltage at a given current. The platinum−ruthenium microstructures of these two electrocatalysts in the fabricated electrodes were characterized by X-ray absorption spectroscopy (EXAFS). EXAFS indicated that there was no Pt−Ru metal−metal interaction in the commercial catalyst; instead, only ruthenium oxide signals were observed. On the other hand, the YZU catalyst contains a Pt−Ru bimetallic interaction as indicated by the X-ray absorption spectra. It was considered that the Pt−Ru alloy structure has better CO tolerance than nonalloy Pt−Ru structure.

Introduction

In terms of the relatively low weight and volume,[1] methanol as direct fuel for polymer-electrolyte-membrane fuel cells (PEFCs) is attractive for portable power source and mobile applications. However, practical uses of direct methanol fuel cell (DMFC) encountered problems including the overvoltage on anodes made from currently available electrocatalysts.[2] A reformer converting liquid fuels such as methanol to hydrogen-rich fuels is regarded as feasible for larger-scale on-site power generation and for electrical vehicles. However, such fuels usually contain ca. 1% CO, and the commonly used carbon-supported platinum-based catalysts are not practical due to their very low CO tolerance (less than 100 ppm) at typical operating temperatures (ca. 373 K) and the large anode overpotential when using reformed hydrocarbon fuels. The anode polarization caused by CO poisoning results in voltage losses in fuel cells, usually attributed to the stronger CO chemisorption on Pt clusters, and consequently inhibition of hydrogen oxidation.[3] Some proposed solutions use gas treatment procedures in either current chemical processes (e.g., water-gas shift reaction) or membrane separation processes (e.g., Pd−Ag membrane) to reduce this CO poisoning effect.[4−6] Alternative proposals such as introducing oxygen (air-bleed) into the hydrogen-rich CO-containing fuels were also found effective by converting CO into CO_2.[7,8] However, the disadvantages of these solutions include increasing the system complexity and side effects such as sintering of the electrocatalysts due to the exothermic reactions of the oxygen with CO and hydrogen at the anodes in the air-bleed technology. Thus, the development of CO-tolerant electrocatalysts is necessary before hydrogen−oxygen PEFCs can be widely applied.

Carbon-supported Pt−Ru catalysts have been shown to be among the best candidates for electrochemical oxidation of methanol at anodes of DMFC[9,10] and seem to be promising electrocatalysts for CO tolerance at the anodes of PEFCs.[11−18] A Pt/Ru atomic ratio of 1:1 was reported as the most CO-tolerant Pt−Ru/C catalysts.[13−15] However, the catalytic performance may be dependent not only on the bulk composition but also on the morphology of the catalyst. To be more specific, the electroactivity and the CO tolerance of a Pt−Ru/C catalyst may be determined by the microscopic chemical structures as well as the local interactions among the two metal components and the support surface. How these structural parameters of a catalyst correlate to its performance in fuel cell applications was not clear at the moment. Tilquin et al. reported that graphite-supported Pt had much more active sites than graphite-intercalated Pt under similar loading and cluster size.[19] It indicated that the local structure of a catalyst could affect its performance. However, the same report showed that both Pt catalysts were equally poisoned by CO. Literature data seem to imply a preference of Pt−Ru alloy phase for CO-containing fuels,[11−18] but no direct evidence was found to infer that the Pt−Ru alloy phase would show better CO tolerance than the mixed phase. Since the EXAFS (extended X-ray absorption fine structure spectroscopy) technique is capable of determining these structural parameters,[20] this study was intended to use it for morphology analyses and the correlation between the morphology and the CO tolerance of different Pt−Ru/C electrocatalysts.

* To whom correspondence should be addressed.

10.1021/jp982296p CCC: $18.00
Published on Web 12/15/1998

Experimental Section

Catalysts and Electrodes Preparation. Two Pt−Ru/C catalysts both with a Pt/Ru atomic ratio of 1:1 were examined in this study. A commercial 20% Pt−10% Ru/C catalyst was used without further treatment. Our synthesized 10% Pt−5% Ru/C catalyst (YZU catalyst) was prepared by sequential deposition from H_2PtCl_6 (Johnson-Matthey, 99.9%) and $RuCl_3$ (Johnson-Matthey, 99.9%) on carbon black (Vulcan, XC-72R) in an aqueous environment at 323 K at a pH of 9 (controlled by the addition of 1 N NaOH from Merck). This catalyst was then subjected to a 4 h reduction at 523 K under flowing H_2. The gas-phase CO and H_2 chemisorption of these catalysts were examined at room temperature using a commercial unit (Micromeritics, ASAP-2000). The anodes for half-cell tests were prepared by dispersing ca. 0.6 g of catalyst powders in a solution containing H_2SO_4 (Merck, GR, 95−97%) and PTFE (duPont, 30%), which was subsequently spread, cold-pressed over a 10 × 10 cm window on a PTFE-treated carbon paper, and then hot-pressed and heat-treated to 623 K.

Electrochemical Half-Cell Measurements. Half-cell performance tests were measured by using a two-compartment electrochemical cell system. An electrode approximately 2 × 2 cm was cut from the sheet and was sandwiched between two compartments. The working electrode area exposed to the electrolyte was only about 1 cm^2. A standard Ag/AgCl electrode (Mettler Toledo) was used as the reference electrode, and a 1 × 1 cm Pt foil was used as the counter electrode. All the reported voltage was corrected with respect to the reversible hydrogen electrode. A cyclic voltammetric scan was typically allowed for at least 1 h at room temperature (300 K) at 5 mV/s with 1 M H_2SO_4 (Merck, GR, 95−97%) as the electrolyte. The counter compartment was empty, and both compartments were constantly purged with nitrogen (San-Fu, 99.995%). Subsequently, half-cell performance tests ($I-V$) were carried out by continuously supplying the counter compartment with either pure H_2 (San-Fu, 99.999%) or CO-containing H_2; the CO composition was adjusted by mixing pure H_2 and 500 ppm of CO/H_2 in suitable proportions. The CO tolerance half-cell tests were carried out at 353 K, and the stabilized polarization voltage after each stepwise increase in the load current was recorded; typically the polarization voltages stabilized within a few seconds after each adjustment of the load current. To ensure that the system was free from the interference due to other gases in the atmosphere, all the gas lines had gas traps in their exits. The potentiostat (Hokuto Denko, HA303) was used together with a function generator (Hokuto Denko, HB-105), and the results were recorded with a computer via a remote A/D converter (Advantech, ADAM).

Membrane Electrode Assembly and Single-Cell Measurements. Anodes for polymer-electrolyte-membrane fuel cells (PEFCs) were prepared by applying either the commercial Pt−Ru/C catalyst or the YZU catalyst on a wetproof carbon paper, followed by calcination under flowing nitrogen at 573 K. The membrane electrode assembly (MEA) was fabricated by impregnating the catalyst layer and hot-pressing onto a Nafion 117 membrane. The cathode catalyst was a carbon-supported platinum (Johnson-Matthey, 20% Pt/C). The electrochemical CO tolerance test was carried out under 100 ppm of CO in hydrogen with water vapor in anode and oxygen with water vapor in cathode at a cell temperature of 353 K.

X-ray Absorption Spectroscopy. Fresh electrodes were examined with the X-ray absorption measurements, which were performed on the X-ray beam line X-11A of The National Synchrotron Light Source (NSLS) at Brookhaven National Laboratory with a storage ring energy of 2.5 GeV and a beam current between 200 and 100 mA. A Si(111) double-crystal monochromator was used for energy selection, and it was detuned 20% at E_0 + 50 eV to suppress higher harmonic radiation. The resolution, $\Delta E/E$, was estimated to be 2.0 × 10^{-4}. The transmission measurement geometry was arranged by using gas-filled ionization chambers to monitor the intensities of the incident and transmitted X-ray through the catalyst samples. The monochromator was scanned in energy from 200 eV below the platinum L_{III} absorption edge (11 564 eV) and ruthenium K absorption edge (22 117 eV), respectively, to 1200 eV above the edge. Due to the energy constraint of the synchrotron light source in Taiwan (SRRC), data at the platinum L_{III} edge only were examined again on both samples.

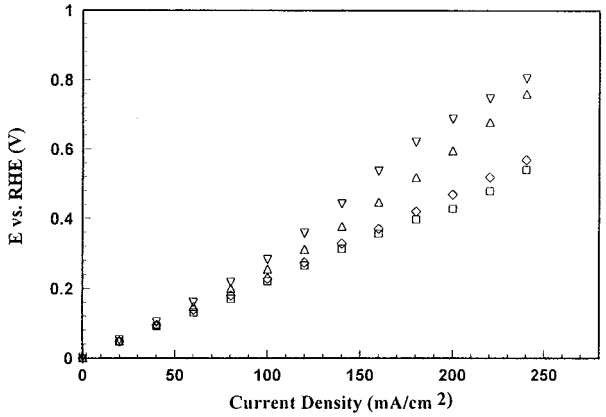

Figure 1. The 353 K anodic half-cell CO tolerance test of the 20% Pt−10% Ru/C commercial catalyst under pure H_2 (□) and 250 ppm of CO in H_2 for 5 min (◇), 15 min (△), and 60 min (▽).

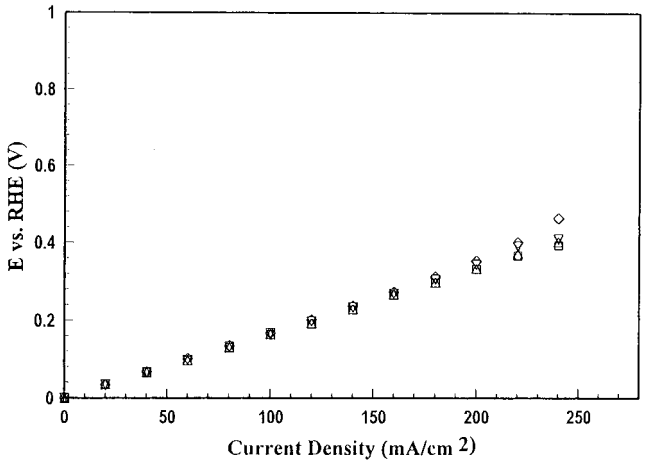

Figure 2. The 353 K anodic half-cell CO tolerance test of the 10% Pt−5% Ru/C YZU catalyst under pure H_2 (□) and 250 ppm of CO in H_2 for 5 min (◇), 15 min (△), and 60 min (▽).

Results

Electrochemical CO Tolerance Tests. The changes in the half-cell $I-V$ spectrum with respect to the onstream time under 250 ppm of CO in H_2 are shown in Figures 1 and 2 for the two catalysts. It was found that continual exposure to CO at a specific current led to an increase in the polarization voltage. Longer CO exposure and higher load currents caused a greater increase in the polarization voltage. The effect of CO exposure time seems to suggest the accumulation of surface CO-induced poisoning species, and the effect of higher load current seems to imply that the formation of CO-induced poisoning species was increased at higher currents.

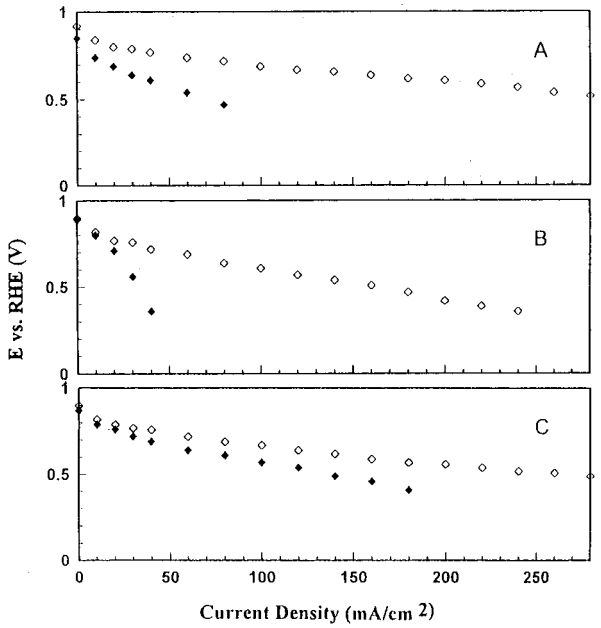

Figure 3. PEMFC single-cell CO tolerance test of (A) the commercial Pt−Ru/C catalyst, (B) the commercial 20% Pt/C catalyst, and (C) the YZU Pt−Ru/C catalyst under pure H_2 (open symbols) and 100 ppm of CO in H_2 for 60 min (filled symbols).

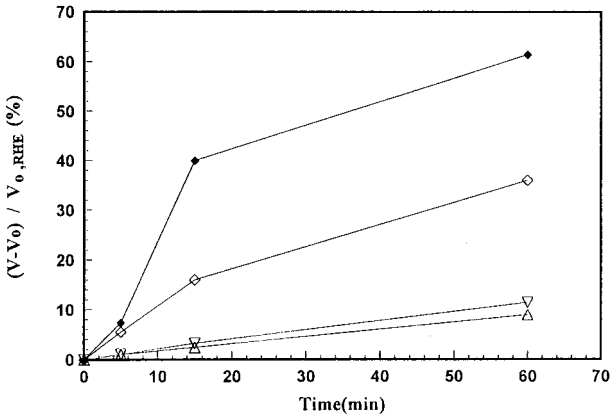

Figure 4. Effect of onstream time on the relative changes of the anodic half-cell potential of the commercial Pt−Ru/C catalyst (◇, ◆) and of the YZU Pt−Ru/C catalyst (△, ▽) under 250 ppm of CO in H_2 at 100 mA/cm^2 (◇, △) and 200 mA/cm^2 (◆, ▽).

Comparing the relative changes in the polarization voltage for the same onstream times and load currents, it can be concluded that the 10% Pt−5% Ru/C YZU catalyst had better CO tolerance than the commercial 20% Pt−10% Ru/C. A similar conclusion was drawn from the single-cell CO tolerance tests shown in Figure 3. The YZU catalyst showed the least decay in the current−voltage curve among the three catalysts studied; the commercial Pt−Ru/C catalyst was less CO tolerant while the commercial 20% Pt/C catalyst showed the highest increase in the polarization voltage under 100 ppm of CO in H_2. Figure 4 compares the relative changes in the half-cell polarization voltage as a function of onstream time and the load current for the two Pt−Ru/C catalysts. The YZU catalyst showed relatively small variations in the polarization voltages and was quite stable over the 1 h test period. To further examine the CO tolerance of the YZU catalyst, the half-cell polarization voltage was recorded over a prolonged period under a 250 ppm CO environment at a constant load current of 60 mA/cm^2; the results are shown in Figure 5. It was observed that this catalyst was quite stable under 250 ppm of CO up to 60 min; however,

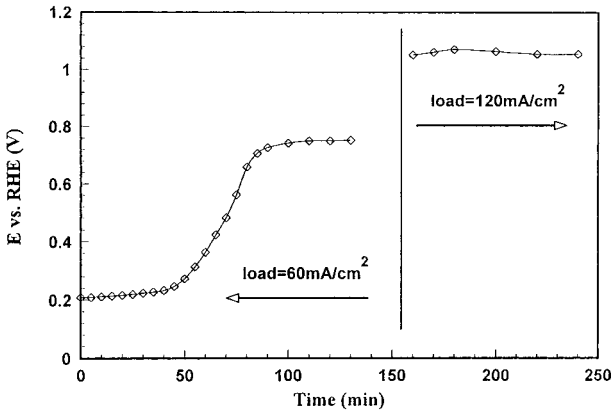

Figure 5. Effect of onstream time on the anodic half-cell potential of the YZU Pt−Ru/C catalyst under 250 ppm of CO in H_2.

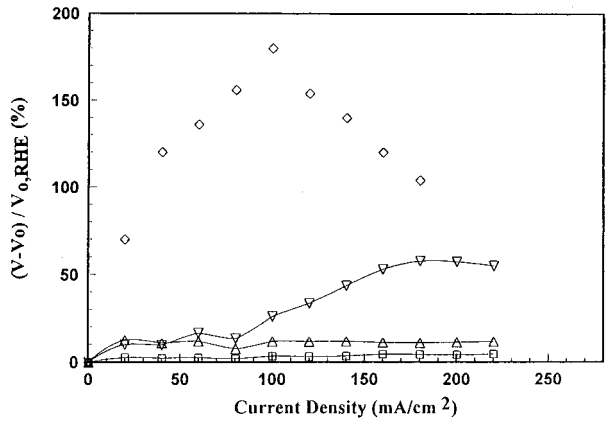

Figure 6. Effect of CO concentration and the load current on the relative changes of the anodic half-cell potential of the commercial Pt−Ru/C catalyst (◇) under 250 ppm of CO in H_2 and of the YZU catalyst under 50 ppm (□), 250 ppm (△), and 500 ppm (▽) CO in H_2.

the polarization voltage rose after 60 min and reached a plateau. A subsequent adjustment to a higher load of 120 mA/cm^2 resulted in a stable polarization voltage for more than 90 min. The reason for the rise to a second stabilized voltage under constant load at 60 mA/cm^2 is not known; however, this catalyst appeared to maintain quite steady performance over a time scale as hours. Figure 6 shows the effects of load current and of CO concentration on the relative changes in the half-cell polarization voltage. Under 250 ppm of CO and load currents below 80 mA/cm^2, both Pt−Ru/C catalysts showed similar CO tolerance, but the YZU catalyst was superior at higher load. However, the performance of our synthesized catalyst deteriorated significantly under 500 ppm of CO.

Gas-phase adsorption experiments of the two Pt−Ru/C catalysts were designed to parallel the electrochemical CO tolerability tests, and it contained a sequence of H_2 chemisorption, 623 K evacuation, CO chemisorption, 623 K evacuation, and another H_2 chemisorption. In each chemisorption step the experiment was carried out at 298 K with a dual-isotherm method where a 30 min evacuation period was allowed between isotherms. The 623 K evacuation was used to desorb all the surface hydrogen and surface CO which has a similar adsorption strength to surface hydrogen. Therefore, by comparing the irreversible uptakes of the first and the second H_2 chemisorption experiments, one can obtain the percentage of surface sites that were occupied by strongly adsorbed CO. Table 1 shows the results of these gas-phase adsorption experiments, and it is obvious that the YZU catalyst had a lower fraction of surface that strongly adsorbed CO.

TABLE 1: Sequential Gas-Phase Chemisorption Studies of the Two Pt−Ru/C Catalysts at 298 K

		irreversible uptake (mmol/g)	
sequence no.	adsorbate	20% Pt−10% Ru/C (commercial)	10% Pt−5% Ru/C (YZU)
1	H_2	92	175
2	CO	303	270
3	H_2	28	88
$uptake_{no.3}$/ $uptake_{no.1}$(%)		30	50

XANES and EXAFS. The EXAFS data were analyzed using mostly experimentally determined reference files obtained from standard materials of known structures; only the Pt−Ru reference file was determined by a theoretical calculation. The Pt−Pt, Ru−Ru, Pt−O, Pt−C, and Rh−O phase shifts and backscattering amplitude were extracted from EXAFS data for Pt foil, Ru powders, $Na_2Pt(OH)_6$, $Ir_4(CO)_{12}$, and Rh_2O_3, respectively. Theoretical calculation of Teo and Lee shows that the amplitude and phase function of the nearest and next-nearest neighbors in the periodic table are almost identical.[21] This justifies the appropriateness of using the Rh−O phase function to represent that of Ru−O. The Pt−C contribution was included for the characterization of metal−support interfaces. This is usually obscured by the stronger contribution from metal particles. To examine this effect, it would require small enough metal particles and good EXAFS data quality. Table 2 lists the results of the quantitative analyses.

A cubic spine background subtraction was used to extract EXAFS data from measured X-ray absorption data.[22] The resulting spectrum was normalized by a division by the edge height to obtain the final EXAFS and XANES. The white line intensity at the Pt L_{III} edge for the YZU catalyst is higher than that found for the commercial catalyst, as shown in Figure 7. The differences in EXAFS functions for both samples characterized at the Pt L_{III} edge and Ru K edge are shown in Figure 8 and Figure 9, respectively. For both samples at the Pt L_{III} edge, there are significant oscillations at values of k (the wave vector) up to about 14 A^{-1}, indicating the formation of Pt and/or Ru−Pt clusters on the carbon support. In contrast, the EXAFS data of the YZU sample indicate the formation of metal−metal bonding, whereas no significant metal−metal contributions were observed for the commercial catalyst. The k^3-weighted Pt−Pt phase and amplitude-corrected Fourier transforms of EXAFS function in r (distance) space are shown in Figure 10. The amplitude of the major peak (at about 2.7 Å) for the YZU catalyst is almost the same as (within experimental error) that for the commercial catalyst, which suggests that the cluster sizes for both catalyst samples have no significant difference.

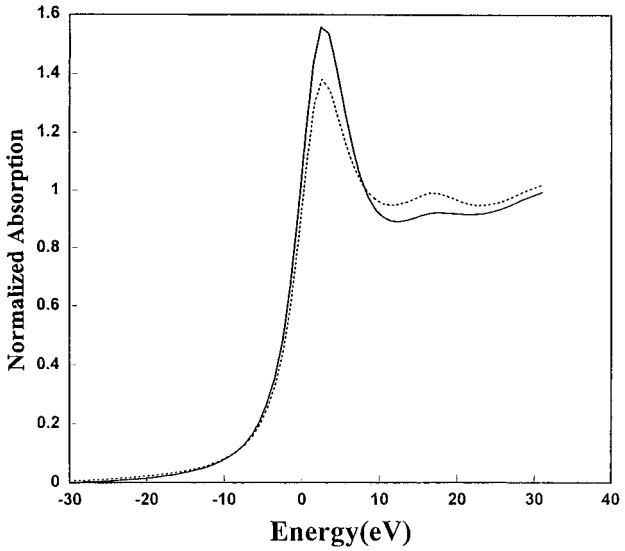

Figure 7. Structure of the Pt L_{III} absorption edge for the commercial Pt−Ru/C catalysts (dashed line) and of the YZU catalyst (solid line).

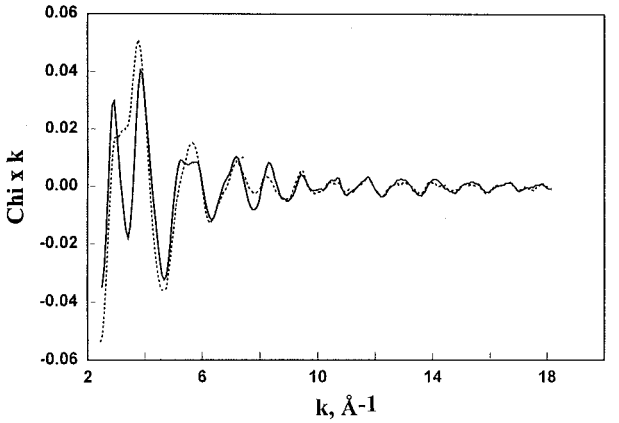

Figure 8. Raw EXAFS data of the Pt edge for the commercial Pt−Ru/C catalyst (solid line) and of the YZU catalyst (dashed line).

Because of the similar bond distance of the Pt−Pt and the Pt−Ru contributions of the YZU catalyst (shown in Table 2), its real and imaginary parts in Figure 10 peak at the same R although bimetallic interactions are involved.

For an X−Y absorber−backscattering pair, peaks that have a positive imaginary part of the phase-corrected EXAFS function are due to the neighbors of Y.[23,24] As show in Figure 11, the Rh−O phase-corrected Fourier transform of the EXAFS function at the Ru edge of the commercial catalyst presents a symmetric peak at 2.05 Å, suggesting oxygen is the backscattering atom

TABLE 2: EXAFS Analysis Results of the Two Pt−Ru/C Catalysts

catalyst	shell	N	R (Å)	$\Delta\sigma^2$	ΔE_0 (eV)
commercial	Pt edge				
	Pt−Pt	2.1 ± 0.1	2.78 ± 0.003	0.000 06 ± 0.000 32	−13.24 ± 0.70
	Pt−O	0.6 ± 0.1	2.06 ± 0.01	−0.00 045 ± 0.001 65	−5.45 ± 2.45
	Pt−C	5.2 ± 0.7	2.50 ± 0.01	0.001 62 ± 0.001 10	15.05 ± 1.51
	Ru edge				
	Ru−O	3.96 ± 0.08	2.05 ± 0.003	0.001 70 ± 0.000 41	−8.65 ± 0.40
YZU	Pt edge				
	Pt−Pt	2.15 ± 0.34	2.77 ± 0.006	0.001 23 ± 0.000 65	−5.41 ± 1.65
	Pt−Ru	0.93 ± 0.34	2.76 ± 0.04	0.009 93 ± 0.004 53	2.62 ± 3.91
	Pt−C	5.86 ± 0.30	2.01 ± 0.005	0.007 09 ± 0.000 74	−0.33 ± 0.60
	Ru edge				
	Ru−Ru	6.37 ± 0.53	2.65 ± 0.004	0.003 64 ± 0.000 54	5.57 ± 0.39
	Ru−Pt	6.22 ± 8.32	2.73 ± 0.10	0.021 55 ± 0.0186	28.39 ± 12
	Ru−O	0.10 ± 0.14	2.16 ± 0.06	−0.013 ± 0.006	10.30 ± 29

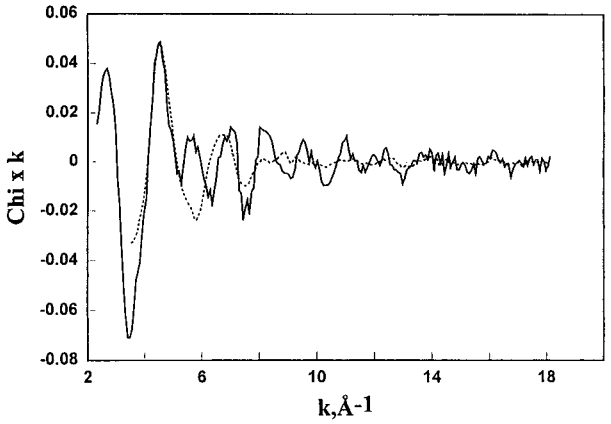

Figure 9. Raw EXAFS data of the Ru edge for the commercial Pt−Ru/C catalyst (dashed line) and of the YZU catalyst (solid line).

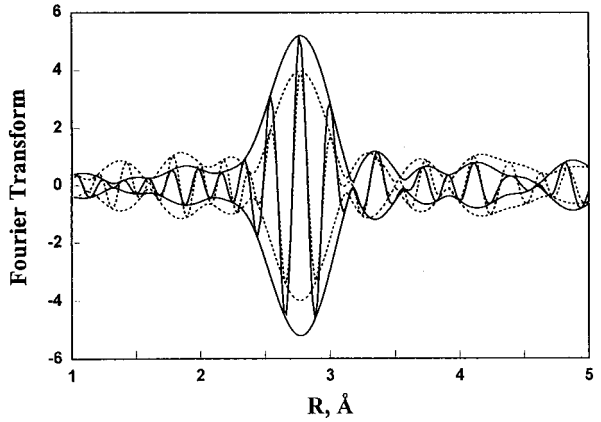

Figure 10. Imaginary part and magnitude of Fourier transform (k^2-weighted, $\Delta k = 9-17$ Å, Pt−Pt phase and amplitude corrected) of Pt edge for the commercial Pt−Ru/C catalyst (solid line) and of the YZU catalyst (dashed line).

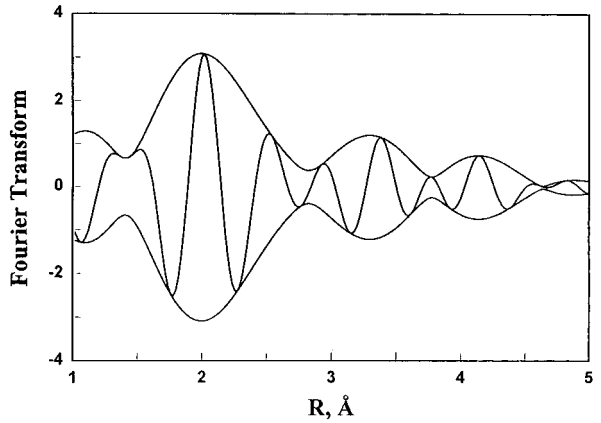

Figure 11. Imaginary part and magnitude of Fourier transform (k^3-weighted, $\Delta k = 4.09-9$ Å, RhO phase and amplitude corrected) of Ru edge for the commercial Pt−Ru/C catalyst.

and the ruthenium oxide is the main species on the carbon support. Fitting was not successful when a Ru−Ru contribution was included. For the YZU catalyst, the Ru−Ru phase and amplitude-corrected Fourier transform of the EXAFS data present a peak appearing at about 2.7 Å. However, the peak is not symmetric, and Table 2 shows that contributions resulting from the Ru−Pt bimetallic interaction, the Ru−Ru, and the Ru−O are involved in the EXAFS data. The bond distance of the Ru−Pt interaction agrees with that of the Pt−Ru from Pt-edge data fitting; this bond distance is slightly shorter than that of Pt−Pt but longer than that of Ru−Ru. The Ru−Pt bond

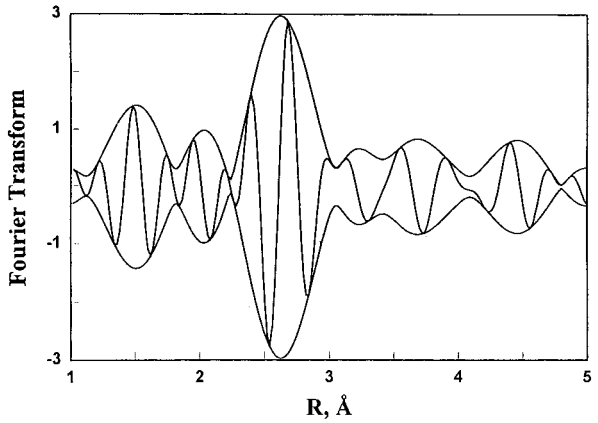

Figure 12. Imaginary part and magnitude of Fourier transform (k^2-weighted, $\Delta k = 7-14$ Å, Ru phase and amplitude corrected) of Ru edge for the YZU Pt−Ru/C catalyst.

distance also agrees within experimental errors to that reported for carbon-supported $PtRu_5$ nanoparticles.[25]

From Figure 7, the white line intensity for the YZU catalyst was significantly higher than that of the commercial catalyst. The intensity of the threshold resonance of the L_{III} edge absorption edge (white line) is related to the transition probabilities of exciting inner-core 2p electrons into vacant d valence levels. The lower the electron density of the metal, the greater the number of vacancies in the valence level and, hence, the higher the probability of the transition.[26] In addition, the Hartree−Fock−Slater LCAO calculation showed a decrease in the d-hole density with increasing size of ionized clusters.[26] It suggests the white line intensity of supported metal catalysts decreases with the increasing cluster size. However, from the comparison of the k^3-weighted Pt−Pt phase and amplitude-function-corrected Fourier transforms of the EXAFS data for the YZU and commercial catalysts (Figure 10), similar cluster sizes and consequently similar white line intensities are expected. The discrepancy between the expected and observed white line intensities may be caused by the Ru−Pt bimetallic interactions. Since the ruthenium oxide was observed for the commercial catalyst, no significant bimetallic interactions were expected for this sample. On the contrary, a significant metal−metal contribution was observed for the YZU catalyst at the Ru K edge. Electron transfers from Pt to Ru caused by bimetallic interactions would result in a lower electron density in Pt and consequently an increase in the white line intensity.

Discussion

The kinetics of hydrogen oxidation on Pt−Ru and other Pt-based bimetallic catalysts is not affected significantly by the presence of a second metal.[27] Thus, the performance of PEMFC by using pure hydrogen/oxygen is expected to be similar for the two Pt−Ru/C catalysts at the present experimental conditions. The metal loading of the catalyst and the utilization of the catalytic surfaces due to the electrode catalyst layer structure usually determine the number of surface atoms available for hydrogen oxidation and consequently the electroactivity. Following identical electrode fabrication procedure, our data suggested that the Pt−Ru loading of these two catalysts could not be attributed as the main reason for their different CO tolerance. Questions concerning whether results obtained in aqueous electrolyte (e.g., 1 M H_2SO_4) in half-cell tests can be applied to fuel cell operating conditions may also be ruled out by the same trend found in single-cell CO tolerance tests. Although both Pt−Ru/C catalysts were at a Pt/Ru atomic ratio

of 1:1, the very different CO tolerance implies that the bulk composition was not the key factor on the CO tolerance. The microstructure in these two catalysts was consequently considered as the determining factor on the CO tolerance. EXAFS results showed that the 10% Pt−5% Ru/C YZU catalyst contained bimetallic interactions suggesting the presence of Pt−Ru alloy phase; on the other hand, the 20% Pt−10% Ru/C commercial catalyst contained mainly mixed Pt phase and Ru phase. The better CO tolerance of the former catalyst implies that the alloy phase may be more CO tolerant than the mixed phases.

CO has been found to result in stronger adsorption than H_2 over group VIII transition metals such as Pt, Pd, Ni, etc. This provides an argument that the CO poisoning effect on the electrooxidation of H_2 is due to the stronger adsorption of CO over active sites. However, gas-phase adsorption results showed that the CO adsorption strength on these transition-metal surfaces was reduced when electronegative additives were present.[28,29] This indicates that the CO adsorption could be weakened when the transition metals such as Pt have lower electron density. The applicability of the gas-phase adsorption results to electrochemical systems was proved previously.[30,31] Therefore, a similar weakening of CO adsorption could be expected in electrochemical systems when Pt has a lower electron density. Based on the EXAFS studies, both the lower white line intensity in XANES in Figure 7 and the structural information in Figure 10 indicated a lower Pt electron density in the YZU catalyst, likely due to the bimetallic interaction of Pt−Ru clusters. The lower electron density of Pt and the better CO tolerance of the YZU catalyst suggest that its better CO tolerance could be induced from lowering the electronic density state of Pt. As a consequence, H_2 molecules could become competitive enough with CO molecules for catalytic sites, and the overall electroactivity was only slightly affected. The gas-phase adsorption results shown in Table 1 also indicate a more competitive adsorption of H_2 with CO on the YZU catalyst; this confirms that the weakened CO adsorption played a role in the CO tolerance mechanism of the YZU catalyst.

Not only is CO adsorbed more strongly, the lower reactivity of the adsorbed CO is generally recognized with its poisoning effect; therefore, strategies for improving the CO tolerance of electrocatalysts for fuel cells lie in either promoting the oxidation of adsorbed CO or weakening the CO adsorption. Experiments on well-characterized Pt−Ru bulk alloy[11−15] implied that alloy-forming Pt−Ru/C catalysts could be considered as the most CO tolerant; this agrees with the better CO tolerance of the alloy-like YZU catalyst. However, previous attributions on these Pt−Ru bulk alloy were mostly to the enhanced oxidation of the adsorbed CO, i.e., the so-called bifunctional mechanism.[11−18] To check for this possibility, the YZU catalyst was subjected to a positive sweep scan after the 1 h CO tolerance test. Almost negligible CO oxidation signal was observed, and therefore the better CO tolerance of the YZU catalyst could be attributed more to the weakening of CO adsorption.

Gastiger et al. discussed the possibility of the weakened CO adsorption on Pt−Ru alloy and questioned whether the CO adsorption strength was increased or decreased.[11] Indeed, a somewhat lower C−O stretching frequency of the irreversibly linearly bonded CO on Pt−Ru than that on Pt observed by Ianniello et al.[14] seems to argue against the weakened metal−CO bonding strength on Pt−Ru in electrochemical systems. However, the significantly lower intensity of the C−O IR band on the Pt−Ru alloy comparing to the polycrystalline Pt under similar conditions[14] implies that a smaller fraction of surface sites was blocked by the strongly adsorbed CO. This agrees with the gas-phase adsorption results in this study; therefore, the weakening of CO adsorption on the Pt−Ru surface should be still possible and may contribute to its CO tolerance. That the CO electroxidation was suppressed on Pt surfaces in the presence of electronegative Cl^- species[32] may cast some doubts about the enhanced CO tolerance of the electron-deficient Pt−Ru/C. However, the weakened CO adsorption over Pt−Ru alloy cannot be excluded from this study and from the previously observed lower C−O IR band intensity and the lower CO_{ad} oxidation potential over $Pt_{0.5}Ru_{0.5}$ and $Pt_{0.7}Ru_{0.3}$ bulk alloy than that on polycrystalline Pt.[14]

Though the bifunctional mechanism including the enhanced oxidation of adsorbed CO was more commonly attributed, it is possible that an enhanced CO tolerance could be induced without an enhancement in the CO electrooxidation. Cooper et al. pointed out that an enhanced CO oxidation typically resulted from the presence of surface oxide such as WO_3 or SnO_2 on Pt surfaces, whereas a modification in the CO/H_2 adsorption behaviors contributed to the higher CO tolerance of binary alloys such as PtRu, PtCo, and PtRh.[33] From this point of view, if the Ru in Pt−Ru/C were in the form of RuO_x, the mechanism of enhanced oxidation of the adsorbed CO may be involved for the CO tolerance of the catalysts. On the other hand, if the Ru in Pt−Ru/C formed an alloy with Pt, the CO tolerance could be attributed to the perturbed CO adsorption. That the EXAFS results of the commercial catalyst revealed the presence of mainly RuO_x indicates the possible involvement of enhanced CO oxidation with this catalyst, but its mechanistic effect on the CO tolerance was not better than the alloy-like morphology of the YZU Pt−Ru/C catalyst. This seems to suggest that the better CO-proof mechanism may be the weakening in the CO adsorption via the reduced Pt electron density. However, no clear comparison could be made if the microstructure were not optimized for either type of Pt−Ru morphology, not to mention the possibility of the coexistence of both types of Pt−Ru morphology in one catalyst.

Although the YZU catalyst showed better CO tolerance, either a prolonged exposure to 250 ppm of CO or a dosing with higher CO content resulted in a quick polarization of the anode. This indicates that there is still a long distance to the development of a practical CO tolerant electrocatalyst. As a speculation from the results of this study, a catalyst fabrication to involve both the weakening of CO adsorption and the promoted CO oxidation may be a good direction to follow. That is to develop a catalyst containing mixed phases of PtRu alloy and surface oxides such as RuO_x. The adsorption of CO is usually a slow process under both kinetic and diffusion control at the anode potentials of PEM fuel cells.[3] The Pt−Ru alloy clusters may have the effect of reducing CO surface coverage via the weakened adsorption strength of CO. The ruthenium oxide or ruthenium metal neighboring to adsorbed CO is capable of promoting CO oxidation by working as an oxygen donor via either hydroxyl groups or adsorbed water.[9] This would consequently release the CO-occupied sites for hydrogen oxidation. The oxidation of CO with oxygen donors may also occur by the Eley−Rideal mechanism (adsorbed oxygen reacts with gas-phase CO) concurrently with the Langmuir−Hinshelwood mechanism (adsorbed CO reacts with adsorbed oxygen) at the anodes in PEM fuel cells. The former mechanism could occur because of the reported electrooxidation of dissolved CO on CO-free Pt surface.[34] Thus, the targeted morphology of Pt−Ru/C may benefit from the synergistic effect of a weaker CO interaction

and a quicker oxidation of adsorbed CO at a lower potential than the H_2 oxidation potential.

Conclusions

Two Pt−Ru/C catalysts at a Pt/Ru atomic ratio of 1:1 were examined for the CO tolerance for applications in fuel cells. The catalyst showing better CO tolerance was found to contain mainly Pt−Ru bimetallic interaction from EXAFS. The other catalyst was found to contain mainly mixed phases of Pt and RuO_x and to have a somewhat lower CO tolerance. The morphology of the Pt−Ru/C catalyst was considered keenly related to the CO tolerance. The catalyst showing bimetallic interactions was also found to have a weakened CO adsorption from the gas-phase adsorption studies, and it was attributed as the mechanistic effect of the catalyst's better CO tolerance.

Acknowledgment. The EXAFS data were analyzed with XDAP Data Analysis Program, developed by M. Vaarkamp, J. C. Linders, and D. C. Koningsberger, and the reference files were provided by Dr. B. C. Gates. This research was supported by the Energy Commission of Minister of Economic Affairs and National Science Council, Republic of China. We are also grateful to the staff of beam line X-11A at the National Synchrotron Light Source, U.S.A., and the X-ray beam of SRRC, the Taiwan light source (TLS), for their assistance.

References and Notes

(1) Hobbs, B. S.; Tseung, A. C. C. *Nature* **1969**, *222*, 556.
(2) Hogarth, M. P.; Hards, G. A. *Platinum Met. Rev.* **1996**, *40*, 150.
(3) Dhar, H. P.; Christner, L. G.; Kush, A. K. *J. Electrochem. Soc.* **1987**, *134*, 3021.
(4) Chen, K. Y.; Shen, P. K.; Tseung, A. C. C. *J. Electrochem. Soc.* **1991**, *38*, 2278.
(5) Jayaraman, V.; Lin, Y. S. *J. Membr. Sci*. **1995**, *104*, 251.
(6) Amphlett, J. C.; Mann, R. F.; Peppley, B. A. *Proceedings of 1st International Symposium on New Materials for Fuel Cell Systems*, Montreal, 1995; p 249.
(7) Kulesza, P. J.; Faulkner, L. R. *J. Electroanal. Chem*. **1989**, *259*, 81.
(8) Campbell, S.; Stumper, J.; Wilkinson, D. *Abstracts of 1997 Joint International Meeting of ECS/ISE*, Paris, 1997; p 87.
(9) Watanabe, M.; Uchida, M.; Motoo, S. *J. Electroanal. Chem*. **1987**, *229*, 395.
(10) Watanabe, M.; Furuchi, Y.; Motoo, S. *J. Electroanal. Chem*. **1985**, *191*, 367.
(11) Gastiger, H. A.; Markovic, N.; Ross, P. N., Jr. *J. Phys. Chem.* **1995**, *99*, 16757.
(12) Gastiger, H. A.; Markovic, N.; Ross, P. N., Jr. *J. Phys. Chem.* **1995**, *99*, 8290.
(13) Gastiger, H. A.; Markovic, N.; Ross, P. N., Jr.; Cairns, E. J. *J. Phys. Chem.* **1994**, *98*, 617.
(14) Ianniello, R.; Schmidt, V. M.; Stimming, U.; Stumper, J.; Wallau A. *Electrochim. Acta* **1994**, *39*, 1863.
(15) Schmidt, V. M.; Ianniello, R.; Oetjen, H.-F.; Reger, H.; Stimming, U.; Trila, F. *Electrochem. Soc. Proc.* **1995**, *95*−*23*, 1.
(16) Oetjen, H.-F.; Schmidt, V. M.; Stimming, U.; Trila, F. *J. Electrochem. Soc.* **1996**, *143*, 3838.
(17) Frelink, T.; Visscher, W.; Cox, A. P.; van Veen, J. A. R. *Ber. Bunsen-Ges. Phys. Chem.* **1996**, *100*, 599.
(18) Watanabe, M.; Motoo, S. *J. Electroanal. Chem*. **1975**, *60*, 267.
(19) Tilquin, J. Y.; Cote, R.; Guay, D.; Dodelet, J. P.; Denes, G. *J. Power Sources* **1996**, *61*, 193.
(20) Sinfelt, J. H.; Via, G. H.; Lytle, F. W. *J. Phys. Chem.* **1978**, *68*, 2009.
(21) Teo, B. K.; Lee, P. A. *J. Am. Chem. Soc.* **1979**, *101*, 2815.
(22) van Zon, F. B. M. A Structural Investigation of Supported Small Metal Particles and Metal-Support Interface with EXAFS. Dissertation, Eindhoven University of Technology, Eindhoven, The Netherlands, 1989; p 18.
(23) Lee, P. A.; Beni, G. *Phys. Rev. B* **1977**, *15*, 2862.
(24) van Zon, F. B. M.; Maloney, S. D.; Gates, B. C.; Koningsberger, D. C. *J. Am. Chem. Soc.* **1993**, *115*, 10317.
(25) Nashner, M. S.; Frenkel, A. I.; Adler, D. L.; Shapley, J. R.; Nuzzo, R. G. *J. Am. Chem. Soc.* **1997**, *119*, 7760.
(26) Ravenek, W.; Jansen, A. P. J.; van Santen, R. A. *J. Phys. Chem.* **1989**, *93*, 6445.
(27) Mukerjee, S.; McBreen, J. *J. Electrochem. Soc.* **1996**, *143*, 2285.
(28) Wimmer, E.; Fu, C. L.; Freeman, A. *J. Phys. Rev. Lett.* **1985**, *55*, 2618.
(29) Crowell, J. E.; Garfunkel, E. L.; Somorjai, G. A. *Surf. Sci.* **1982**, *121*, 303.
(30) Bett, J.; Kinoshita, K.; Routsis, K.; Stonehart, P. *J. Catal.* **1973**, *28*, 160.
(31) Tran, T. D.; Langer, S. H. *Anal. Chem*. **1993**, *65*, 1805.
(32) de Becdelievre, A. M.; de Becdelievre, J.; Clavilier, J. *J. Electroanal. Chem*. **1990**, *294*, 97.
(33) Cooper, S. J.; Gunner, A. G.; Hoogers, G.; Thompsett, D. *Proceedings of the 2nd International Symposium on New Materials for Fuel Cells and Modern Battery Systems*, Montreal, 1997.
(34) Couto, A.; Perez, M. C.; Rincon, A.; Gutierrez, C. *J. Phys. Chem*. **1996**, *100*, 19538.